Phospholipid Membranes Decorated by Cholesterol-Based Oligonucleotides as Soft Hybrid Nanostructures

Martina Banchelli,[‡] Francesca Betti,[‡] Debora Berti,*[,‡] Gabriella Caminati,[‡] Francesca Baldelli Bombelli,[‡] Tom Brown,[†] L. Marcus Wilhelmsson,[§] Bengt Nordén,[§] and P. Baglioni*[,‡]

Department of Chemistry and CSGI, University of Florence, Via della Lastruccia 3, Sesto Fiorentino, 50019 Florence, Italy, , Department of Chemical and Biological Engineering, Physical Chemistry, Chalmers University of Technology, SE-41296 Gothenburg, Sweden, , School of Chemistry, University of Southampton, Highfield, Southampton SO17 1BJ, U.K.

Received: March 19, 2008; Revised Manuscript Received: May 16, 2008

DNA monomers and oligomers are currently showing great promise as building blocks for supramolecular arrays that can self-assemble in a fashion preprogrammed by the base pairing code. The design and build-up of hybrid DNA/amphiphilic self-assemblies can expand the range of possible architectures and enhance the selectivity toward a well-specified geometry. We report on the self-assembly properties in aqueous solution of a cholesteryl−tetraethylenglycol single stranded 18-mer oligonucleotide (ON_1TEG-Chol) and on its spontaneous insertion in fluid phospholipid membranes. Up to 500 units of these lipophilic ss-oligonucleotides can be incorporated in the outer leaflet of 350 Å radius POPC vesicle. The insertion and hybridization with the complementary oligonucleotide are monitored through light scattering as an increase of hydrodynamic thickness, which is interpreted in terms of average distance between anchoring sites. The conformation of the ss-oligonucleotidic portion is strongly dependent on surface coverage, passing from a quasi-random coil to a more rigid configuration, as concentration increases. Interestingly, conformational details affect in a straightforward fashion the hybridization kinetics. Liposomes with single- and double-strand decorations remain stable within the experimental time window (about one week). The structure represents an example of successful and stable amphiphile/DNA supramolecular hybrid, where a DNA guest is held in a membrane by hydrophobic interactions. The lipophilic oligonucleotide under investigation is therefore a suitable building block that can effectively serve as a hydrophobic anchor in the fluid bilayer to assemble supramolecular constructs based on the DNA digital code.

Introduction

Amphiphilic self-assembly is an attractive bottom-up strategy to produce materials and devices with control at the nanometer length scale. The main advantage over traditional supramolecular covalent architectures lies in the thermodynamic control (and therefore reversibility) of size and shape of the resultant nanostructures and the facile preparation.[1,2] These characteristics can be further exploited through the appropriate incorporation of complex structural motifs in the amphiphilic building blocks. Specific functions can be encoded in the molecular subunits to engineer supramolecular functional constructs with predictable size, shape and physical properties. This approach has led to the relatively new field of functional surfactants, where additional control parameters (i.e., thermoresponsivity, photosensitivity, redox activity, etc.) can be chemically included in the amphiphile.[3,4]

Among the many examples of structural motifs from Nature, DNA monomers and oligomers stand out as the best choice. They are currently showing great promise due to their chemical stability, well understood and predictable physico/chemical properties and highly selective molecular recognition code. These properties, together with the natural occurrence of enzymes that interact with these biopolymers with great specificity (e.g., restriction endonucleases) open up the possibility of building 2-D and 3-D networks with addressability at the Å scale.[5] Some of the authors of this paper have recently devised a strategy for self-assembly of DNA networks using linear and novel branched three-way oligonucleotide building-blocks, and the formation of the fundamental cell of the network, a DNA hexagon with 4 nm sides (the smallest so far reported) has been demonstrated.[6]

The spontaneous self-organization of amphiphiles can be integrated with this naturally inspired strategy through conjugation of oligonucleotides to amphiphilic assemblers to yield building blocks with tailored properties for controlled self-assembly.

We have pioneered the investigation of self-assemblies of phospholipid-based anionic nucleolipids,[7−11] where one single RNA base is enzymatically attached to the polar head of a lecithin, substituting a choline headgroup. Both hydrophophic portions and bases have been changed in order to build self-assembled objects decorated by nucleic functionalities with varying interfacial curvature and chemical selectivity. Recently the evidence of binding of polynucleotides to small globular micelles formed by 1,2-dioctanoylphosphatidyladenosine[12] and of the sandwiching and ordering of polynucleotides and oligo-

* Corresponding authors. E-mail: (P.B.) baglioni@csgi.unifi.it; (D.B.) berti@csgi.unifi.it.
‡ Department of Chemistry and CSGI, University of Florence.
† School of Chemistry, University of Southampton.
§ Department of Chemical and Biological Engineering, Physical Chemistry, Chalmers University of Technology.

10.1021/jp802415t CCC: $40.75
Published on Web 08/09/2008

SCHEME 1: Chemical Structure and Simple Geometric Representation of ON_1TEG-Chol Showing TEG-Chol Attached to the 5′-Thymidine Nucleotide[a]

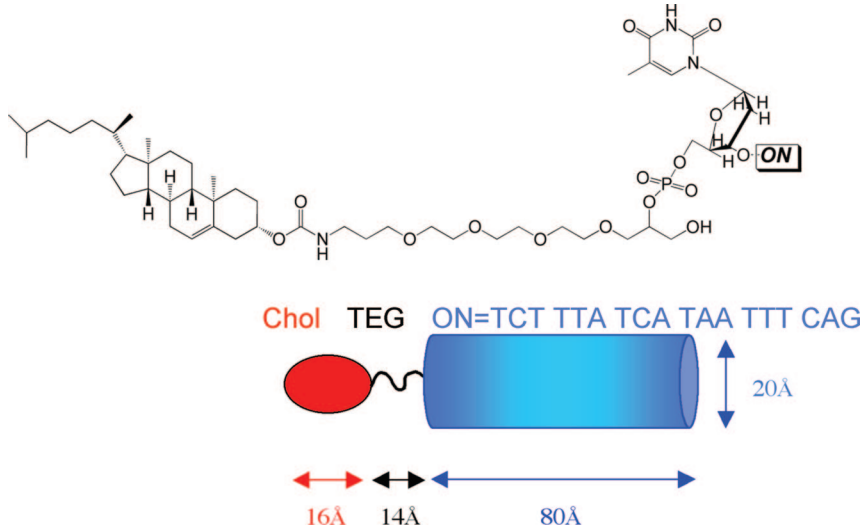

[a] The molecular size was estimated assuming a compact shape and using the contour lengths for the TEG[23] and oligonucleotidic moieties.[24−26] The order of magnitude of the oligonucleotide cross-section is coarsely estimated as the diameter of a B-DNA double helix.

nucleotides between lamellar phases of 1-oloeyl, 2-palmitoylphosphatidyladenosine have been reported.[13] These examples demonstrate that fluid amphiphilic interfaces can induce base pairing processes between amphiphilic single-base derivatives promoting the interaction with similarly charged oligonucleotides. However, the molecular recognition motif of nucleolipids (one single base) is too short to efficiently serve as a building block for DNA-based supramolecular chemistry.

The binding of chemically modified oligonucleotides to "hard" nanoparticles and their subsequent hybridization has been used as a tool to organize nanoparticles into arrays.[14,15] More challenging is the anchoring of oligonucleotides to soft surfaces, such as phospholipid bilayers, that can be either planar (SLM, supported lipid membranes) or curved (liposomes). Such amphiphilic self-assemblies can serve as scaffolds to provide structural skeletons, enhanced local concentration, and/or immobilization and/or favorable orientations for the guest oligonucleotides.

More recently, in the framework of DNA-based nanotechnology, the same derivatives have attracted considerable attention from material scientists as possible building blocks to form supramolecular structures with amphiphilic support. Xu and coauthors have reported an interfacial characterization of cholesteryl−oligonucleotides and demonstrated their incorporation at fluid interfaces.[16] The same derivatives (with different ss-oligonucleotides) have been incorporated in planar membranes by Höök and co-workers and hybridization and tethering of vesicles decorated with the complementary sequence has been achieved.[17] More recently, Boxer and co-workers used lipophilic oligonucleotide pairing to tether intact liposomes to solid-supported planar bilayers.[18]

Some authors have reported that if a linker (PEG, $n = 100$) is inserted between the cholesteryl anchor and the oligonucleotides, the derivative can insert in a negatively charged membrane and hybridize with the complementary unmodified oligonucleotide.[19]

We have designed and characterized a family of amphiphilic oligonucleotides, whose first member is a cholesteryl-tetraethylenglycol single stranded 18-mer oligonucleotide, henceforth called ON_1TEG-Chol. Our aim is to identify a robust anchor for the insertion in a lipidic environment. Therefore we have varied both the degree of hydrophobic functionalizations (one or more cholesterol), their position within the sequence, and the length of the hydrophilic spacer, to test the affinity for the bilayer and the hybridization efficiency.[20] The insertion of the hydrophobically modified oligonucleotide in a lipid bilayer is the first step to build-up more complex DNA-based architectures supported onto membranes. The knowledge of the vesicle loading capacity of DNA, the conformation of the oligonucleotidic portion and its accessibility for biorecognition of the complementary strand in solution are fundamental to produce digitally addressable architectures.

The adsorption of this ON_1TEG-Chol onto hydrophobic SU-8 surfaces and subsequent hybridization has been recently reported.[21,22]

In this paper we investigate the aggregation and surface properties of the ON_1TEG-Chol and characterize its insertion into liquid crystalline bilayers, as a function of surface coverage. The hybridization with the complementary nonhydrophobic oligonucleotide (ON_2-FAM) is also studied both from a kinetic and a thermodynamic point of view. The results are discussed in terms of the oligonucleotide conformation influenced by its lipophilic anchoring in a bilayer.

This paper is organized as follows: (i) the experimental results on the self-assembly of ON_1TEG-Chol in solution are presented; (ii) the insertion of the lipophilic oligonucleotide in a model bilayer is investigated through scattering and spectroscopic techniques as a function of time, concentration and temperature; (iii) the hybridization with the complementary sequence has been monitored with the same techniques.

Experimental Methods

Synthesis of Cholesterol-TEG-ss-DNA-18mers (ON_1TEG-Chol) and ss-DNA-18mer FAM (ON_2-FAM). Standard DNA phosphoramidites, solid supports and additional reagents including the 5′-FAM monomer (6-fluoresceinamidohexyl phosphoramidite) were purchased from Link Technologies and Applied Biosystems Ltd. The cholesterol-TEG phosphoramidite monomer was purchased from Glen Research Inc. An Applied Biosystems 394 automated DNA/RNA synthesizer was used and multiple 1.0 μMole phosphoramidite cycles of acid-catalyzed

detritylation, coupling, capping and iodine oxidation were employed to produce the required oligonucleotides on large scale.[27] 5′-Cholesterol-TEG-modified oligonucleotides and 5′-FAM-modified oligonucleotides were synnthesized "trityl-on" and unmodified oligonucleotides were synthesized "trityl-off". Normal monomers (A, G, C, and T) were allowed to couple for 25 s and the cholesterol-TEG and FAM monomers for an additional 300 s. Stepwise coupling efficiencies and overall yields of monomers were determined by measuring trityl cation conductivity and in all cases these were >98.0%. Cleavage of the oligonucleotides from the solid support was carried out in concentrated aqueous ammonia at 55 °C for 6 h. After ammonia deprotection the cholesterol-TEG oligonucleotides were evaporated to dryness then treated with acetic acid/water (80/20) for 30 min at room temperature to remove the DMT-group from the cholesteryl moiety. After evaporation of the solvent the oligonucleotides were dissolved in water (2.5 mL), extracted with diethyl ether (3 × 5 mL) then purified by reversed-phase HPLC. All other oligonucleotides were purified by reversed-phase HPLC directly after ammonia deprotection and evaporation of aqueous ammonia (HPLC results are available as Supporting Information).

Purification of Oligonucleotides. Purification of oligonucleotides was carried out by reversed phase HPLC on a Gilson system using a Brownlee Aquapore column (C8), 8 mm × 250 mm, pore size 300 Å. The following protocol was used: run time 30 min, flow rate 3 mL per minute, binary system gradient (time in minutes (% buffer B);0 (0); 3(0); 5(20); 21 (100); 25(100); 27 (0); 30(0)). Elution buffer A: 100 mM ammonium acetate, pH 7.0, buffer B: 100 mM ammonium acetate with 70% acetonitrile pH 7.0 (cholesterol-TEG oligomers), buffer B: 100 mM ammonium acetate with 25% acetonitrile pH 7.0 (unmodified and FAM oligomers). Elution was monitored by ultraviolet absorption at 295 nm. After HPLC purification, oligonucleotides were desalted using disposable NAP 10 Sephadex columns (Pharmacia) using the manufacturer's instructions, aliquoted into Eppendorf tubes and stored at −20 °C in distilled deionized water.

Phospholipid Vesicles. POPC (1-palmitoyl-2-oleoyl-*sn*-glycero-3-phosphocholine) was purchased from Avanti Polar Lipids Inc. (Alabama) and used as received. All other chemicals (TRIS base, NaCl) were purchased from Fluka, (Milan, Italy) and used as received. Vesicles were prepared by evaporation of the solvent from a $CHCl_3$/MeOH solution of the lipid; the dry lipidic film was solvated by addition of a 50 mM TRIS, 100 mM NaCl (pH 7.5, TBS) solution. The suspension was vortexed,, frozen−thawed (liquid nitrogen−40 °C water bath) six times and sized down by repeated extrusion (extruder by Lipex Biomembranes Inc., Vancouver, Canada) through stacks of Nucleopore polycarbonate membranes (200, 100 and 50 nm pore size), yielding a narrow sized distribution of unilamellar vesicles. Different liposomal preparations resulted in slightly different initial sizes, hydrodynamic radii ranging from 330 to 350 Å. The total membrane area and the number of lipid molecule in the outer leaflet were determined from the hydrodynamic radius considering an area per POPC of 70 Å^2,[28] and a membrane thickness of 40 Å, for the bilayer in the liquid crystalline state, respectively.

Phospholipid Vesicles Decorated with Oligonucleotides. A stock vesicular dispersion was diluted to 1.3 mM with ON_1TEG-Chol/TRIS buffer varying ON_1TEG-Chol concentration in the diluting buffer. The samples considered, with different lipid/ON_1TEG-Chol ratios, are summarized in Table 1. To test hybridization, the complementary sequence, ON_2-FAM was also added in a 1:1 ratio with respect to the cholesteryl−oligonucleotide. ON_1TEG-Chol translocation across the bilayer during the experimental time window (5 days) is negligible.[29]

TABLE 1: Composition of the Lipid/ON_1TEG-Chol Samples[a]

ON_1TEG-Chol [μM]	$\langle N \rangle$	$\Gamma^{-1/2}$ [Å]
0.3	9	410
2.0	60	158
4.1	125	110
8.3	250	78
16.6	500	55
17.5	525	53
57.0	1700	30

[a] POPC has a fixed concentration of 1.3 mM. The mean occupancy number $\langle N \rangle$ is defined as the average number of ON_1TEG-Chol per liposome. To evaluate $\Gamma^{-1/2}$, the average distance between anchoring sites, the cholesteryl−oligonucleotides have been considered only in the outer vesicular leaflet.

The distribution of guest molecules among colloidal hosts follows a Poisson distribution.[30] Since $\langle N \rangle$ is quite high, the probability of oligonucleotide occupancy $P(\langle N \rangle)$ can be well approximated by a Gaussian distribution function centered at $\langle N \rangle$. If we consider that the oligonucleotide derivative is entirely distributed in the outer vesicular leaflet, and therefore consider the stoichiometry with respect to POPC in the outer leaflet, the knowledge of liposomal size and the narrow size distribution allow a fairly accurate estimate of this number. These $\langle N \rangle$ values, reported in the second column of Table 1, can be converted into an "average distance" ($\Gamma^{-1/2}$) between anchoring sites onto vesicular surface. It should be stressed here that anchoring is due to intermolecular interactions of hydrophobic nature between the cholesterol of the ON_1TEG-Chol and the phospholipid bilayer.

Membrane Incorporation. A quantitative determination of the ON_1TEG-Chol incorporation in lipid bilayer was assessed by gel-filtration on Sephadex G-50 (Pharmacia Fine Chemicals, Uppsala, Sweden). The liposomes were separated from unincorporated ON_1TEG-Chol by a mini-column centrifugation method,[31] which has the advantage that the liposomes can be recovered without dilution. This method is appropriate for separating ON_1TEG-Chol (M_W = 6193) from larger POPC liposomes (~30000 KDa), but it should be mentioned that possible ON_1TEG-Chol oligomers are also excluded.

The Sephadex powder (10 g) was hydrated with 120 mL of TBS and stored for 24 h at 4 °C before use. The mini-column gel filtration was performed under the same conditions on three different samples simultaneously: POPC liposomes and ON_1TEG-Chol (4.1 μM, $\langle N \rangle$= 125), POPC liposomes as a blank, free ON_1TEG-Chol as a control. Fractions of 0.2 mL were collected and subjected to light scattering and UV analysis in order to quantify ON_1TEG-Chol concentration relatively to liposomes. QELS measurements confirm that liposomes are recovered in the first fraction eluted with virtually no dilution (same value of the intensity of scattered light). The light scattering contribution to the UV absorption spectra was evaluated by polynomial fitting of the absorption curve ($\ln(I/I_o) = C\lambda^{-s}$) in the spectral region between 600 and 350 nm, where no absorption from the nucleobases is expected.[32]

Figure 1 shows the results for ON_1TEG-Chol 4.1 μM. The first fraction eluted from the mixed liposome-ON_1TEG-Chol system contains the major amount of ON_1TEG-Chol, (95.8%), almost absent in the subsequent fractions. The 4.2% loss can be due to some free monomers entrapped inside the gel pores that are partially recovered by repeating the elution. The control

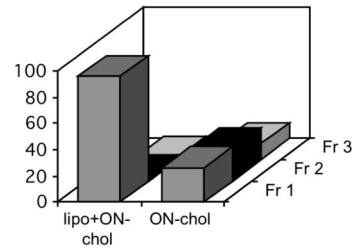

Figure 1. Relative values of UV Absorbance % at 263 nm of the three filtered fractions (Fr 1, Fr 2, Fr 3) with respect to the absorption values before filtration. Left column: liposome-ON_1TEG-Chol. Right column: ON_1TEG-Chol.

experiment performed with ON_1TEG-Chol/TBS shows that 26.5% is inside the first eluted fraction, consistent with the occurrence of some aggregates which do not obviously form in the presence of liposomes.

The presence of liposome therefore significantly alters the relative abundance of ON_1TEG-Chol monomers/oligomers. However, as already highlighted the relatively low cutoff of the pore size is sufficient to exclude dimers, we should mention that the exact nature of such aggregates cannot be determined by this experiment.

Quasi Elastic Light Scattering. QELS experiments were carried out with a Brookhaven Instrument apparatus, New York, USA (BI 9000AT correlator card and BI 200 SM goniometer). The signal was detected by an EMI 9863B/350 photomultiplier. The light source was the doubled frequency of a Coherent Innova diode pumped Nd:YAG laser, ($\lambda = 532$ nm, 20 mW), or alternatively a JDS Uniphase He−Ne ($\lambda = 633$ nm, 5 mW). The laser long-term power stability was ±0.5%. Self-beating detection was recorded using decahydronaphthalene (thermostatted by a water circulating system) as index matching liquid. A temperature probe was inserted in the sample to monitor T while simultaneously recording autocorrelation functions. A control experiment in the same temperature range explored for melting curves has been performed with an aqueous latex dispersion normally used as a standard for QELS calibration. Measurements have been performed in the range 15−55 °C on 0.5 mL samples previously transferred into cylindrical Hellma scattering cells and flushed with N_2 to avoid bubble formation. For each sample at least four separate measurements were performed at three different angles (i.e., 70, 90 and 120° respectively) corresponding to three different scattering vectors $q = 4\pi n/[\lambda \sin(\theta/2)$; n is the refractive index of the medium equal to 1.33. The data analysis was performed as described elsewhere.[11]

Stopped Flow Experiments. The time evolution of the 260 nm absorbance after mixing the oligo-loaded vesicles with the complementary strand solution, was followed with an Applied Photophysics stopped-flow instrument. At least three traces were recorded for each concentration. In order not to saturate the signal and to explore a meaningful range of liposomal coverage, the oligonucleotide concentration has been kept constant at 2 μM, while the lipid content has been varied between 0.125 and 4 mg/mL to scan the interval between 15 and 440 oligos in the outer leaflet respectively. The hybridization rate of a nonliposomal sample for the same oligonucleotide concentration has been also measured as a reference. These solutions were mixed (within approximately 10^{-3} s) via syringe injection into a 1 cm path-length cuvette in a stopped-flow apparatus and hybridization was monitored at fixed temperature, i.e. 25 °C.The time course of the absorbance was recorded between 0.5 to 20 s from time 0, i.e. when the injected solution volume reaches the instrumental beam height in the cuvette.

ζ Potential. The electrophoretic mobility of the vesicles (plain and decorated with ss and ds oligonucleotides) in TBS was determined with a Zetasizer Nano ZS (Malvern Instruments).

Fluorescence. Steady-state fluorescence was measured with a LS50B spectrofluorimeter (Perkin-Elmer, Italy). The fluorescence spectra of pyrene were recorded in the corrected spectrum mode with excitation wavelength set at 335 and 2.5 nm slit, at least 10 scans were averaged for each spectrum. The ratio of the intensities I_1/I_3, which reflects the local polarity sensed by the fluorophore in the organized system,[33] was determined from the first (372 nm) and the third (382 nm) vibronic peaks of pyrene emission spectrum. Pyrene concentration is 1 μM in all samples.

UV−Vis Absorption. UV−vis spectra were recorded with a Lambda 900 spectrophotomer (Perkin-Elmer, Italy) and a Cary 100 spectrometer (Varian, Italy). Thermal cycles from 10 to 70 °C were performed at 0.5 or 0.1 °C/min.

Linear Dichroism. UV−vis linear dichroism (LD) measurements were recorded on a JASCO J-720 CD spectropolarimeter equipped with an Oxley prism to obtain linearly polarized light.[34] Spectra were recorded from 200 to 450 nm in a Couette cell (path length 1 mm) with a shear gradient of 3100 s^{-1} and without applied shear (no orientation of the sample) subtracted as baseline. Isotropic absorption of the same samples was measured on a Cary 4000 (Varian, Italy) spectrophotometer.

LD is defined as the difference in absorption of linearly polarized light and perpendicular polarized light relative to a macroscopic orientation axis (flow direction).

$$\mathrm{LD} = A_{||} - A_{\perp} \quad (1)$$

To observe linear dichroism, a sample oriented with respect to the incident light is required. Liposomes in a Couette cell, subjected to a nearly constant flow gradient, are slightly deformed into elongate ellipsoid-shaped particles that will position their axes preferentially along the flow direction, thereby orienting bound molecules.[35]

Flow LD experiments were measured in 50% w/w buffered sucrose solution at [POPC] = 0.17 mM at different lipid/ON_1TEG-Chol ratios ($\langle N \rangle$ = 125, 250, 500), ON_2-FAM was also added in a 1:1 ratio with respect to the cholesterol−oligonucleotide. The sucrose addition matches the refractive index of the liposome solution reducing the unwanted scattering effects and also provides a better alignment of the particles increasing the viscosity of the solution.[34] Retinoic acid was added as an internal reference ([POPC]/[ret.ac.] = 100:1) to establish the degree of orientation of the liposomes and hence their orientation parameter.[36,37] Provided that the orientation parameter of the system is known, from the reduced linear dichroism, LD^r, defined as the ratio between LD and isotropic absorption, it is possible to evaluate the tilt angle of the molecule with respect to the membrane surface.[38]

Results and Discussion

ON_1TEG-Chol: Aggregation in Aqueous Medium. Figure 2 shows the intensity of scattered light at 90° with respect to the incoming beam, normalized by toluene scattering in the same conditions, as a function of the oligonucleotide concentration. In the same plot, the results obtained using pyrene as a fluorescent probe are also shown.

The scattering intensitiy curve shows a clear slope change as the concentration is raised. For amphiphilic solutions this behavior marks the onset of aggregation. This trend is consistent with the presence of scattering particles in the concentration range 15 μM/800 μM, but we cannot rule out the occurrence

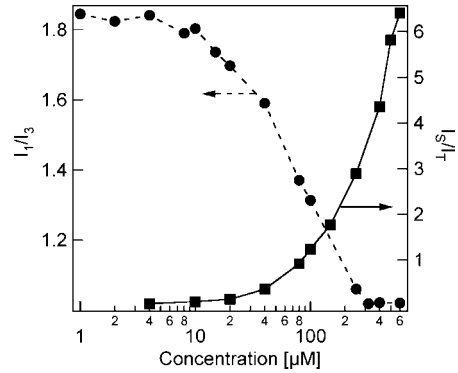

Figure 2. Normalized scattered intensity (squares) and pyrene fluorescence intensity ratio I_1/I_3 (circles) as a function of ON_1TEG-Chol concentration in aqueous solution.

of oligomers, with little contribution to scattering, in the "premicellar" region.

This result is closely correlated with the decrease of I_1/I_3 ratio of pyrene emission, where the aggregation process is monitored through a change of the polarity of the microenvironment sensed by the fluorophore. Therefore, the decrease of I_1/I_3, corresponds to the increase in hydrophobic sites available for pyrene solubilization and hence the formation of aggregates where pyrene can be suitably hosted. The behavior of I_1/I_3 as a function of ON_1TEG-Chol concentration shows a slow decrease for concentration higher than 15 μM, typical of multistep process. This pattern is reminiscent of the well-known bile salt aggregation model: bile salts self-associate in water in small primary aggregates which increase as a function of concentration to form larger secondary aggregates[39] whose size and number increase as a function of concentration.[40]

When pyrene is fully associated with the ON_1TEG-Chol aggregate, i.e. for [ON_1TEG-Chol] > 200 μM, we found $I_1/I_3 = 1.02$ suggesting that pyrene resides closer to the cholesterol groups. In fact, in the case of micelles of tetraethyleneglycol-monoether a value of $I_1/I_3 = 1.30$ was reported[41] whereas lower values ($I_1/I_3 = 0.8$) were found for bile salts derivatives.[40] The micropolarity (μP) sensed by the pyrene probe in the ON_1TEG-Chol aggregate can be estimated from pyrene polarity scales reported in the literature.[42] We found that μP decreases from the value of 62 found in buffer solution to 18 when it is inserted in the aggregate, corresponding roughly to the polarity of short chain alcohols such as butanol.

Interestingly, when a different fluorescent probe was used, i.e., aminonaphtalene sulfonate (ANS), we did not observe any dependence of ANS emission properties on ON_1TEG-Chol concentration, indicating that the crowding of the oligonucleotide sequences hinders penetration of the probe in the hydrophobic pocket of the aggregate.

A more detailed picture of the microstructure of the aggregates can be obtained by QELS, that has been performed in the concentration range 20−800 μM. Below this concentration limit, due to the low scattering contrast, correlation functions have a poor signal-to-noise ratios and QELS results become unreliable.

An analysis of the autocorrelation functions reveals that the decay is invariably bimodal in this concentration range. An angular scan confirms the linear scaling of the relaxation rate with q^2, i.e., the diffusive nature of both modes that contribute to the relaxation of refractive index fluctuations. This result rules out the possible observation of internal motions in the scattering experiment and can be interpreted as the possible simultaneous observation of "micelle-like" aggregates and ON_1TEG-Chol oligomers/monomers.

TABLE 2: Diffusion Coefficients (D) and Hydrodynamic Radii (R_h) As Obtained by Biexponential Analysis of the Autocorrelation Functions for Different ON_1TEG-Chol Concentrations

ON_1TEG-Chol [μM]	D_1 [$\times 10^8$ cm^2 s^{-1}]	R_{1h} [Å]	D_2 [$\times 10^7$ cm^2 s^{-1}]	R_{2h} [Å]
700.0	4.29 ± 0.5	571 ± 3	3.10 ± 0.4	79 ± 3
500.0	4.83 ± 0.3	507 ± 2	3.76 ± 0.4	65 ± 2
250.0	6.45 ± 0.7	380 ± 2	5.33 ± 0.7	46 ± 2

Therefore the correlation functions have been modeled as biexponential decays. The fast decay is attributed to concentration fluctuations of oligomers/monomers, while the slow decay originates from center-of-mass aggregate motions. The diffusion coefficients can be correlated to hydrodynamic radii, according to the Debye−Stokes−Einstein relation

$$D = \frac{k_B T}{6\pi\eta R_h} \tag{2}$$

but a connection to geometric molecular parameters requires implicit assumptions about molecular shape in aqueous solution (rodlike, ellipsoidal and so on), which currently is difficult to accurately define.[43] Table 2 reports the results obtained with this approach.

For the ON_1TEG-Chol oligomers, we obtain an R_h of 45−80 Å, while the "micelle-like" aggregates range from 380 to 600 Å, both sizes increasing with concentration. A comparison with the molecular length scale (see Scheme I) reveals that the aggregates should be highly asymmetric. We do not speculate here on their shape and its concentration dependence. We should stress that the relative amplitudes of the two modes, which are practically invariant in this concentration range, are intensity-weighted (i.e., scaling with R_h,[6] with R_h the characteristic size of the scatterer) and therefore the relative abundance of the two populations should be renormalized by that scaling.

To summarize, some important findings derive from the combination of QELS, pyrene-probe emission on binary ON_1TEG-Chol/TBS systems. Surface tension measurements (Supporting Information) reveal that ON_1TEG-Chol spontaneously adsorbs at the air/water interface. QELS and pyrene-probe emission indicate that below 15 μM the composition of binary solutions mainly consists of monomers or oligomers with a loose hydrophobic core, while above this threshold polydispersed aggregates start to give a measurable contribution to QELS functions.

Insertion of ON_1TEG-Chol into Liposome Bilayer. As discussed in the Introduction, the insertion of a lipophilic oligonucleotide in a liquid-crystalline bilayer should provide distinctive advantages in the build-up of DNA-based hierarchical architectures both with respect to bulk solution self-assembly[44] and with respect to thiol-mediated covalent capture on gold nanoparticles.[45−47]

The driving force for insertion into the lipid bilayer is due to the hydrophobic effect, due to noncovalent interactions. POPC membranes are fluid at room temperature, and therefore guests can redistribute and readjust in a responsive fashion as external parameters are varied (i.e., temperature, salinity, liposomal or ON_1TEG-Chol concentrations, i.e. steric hyndrance). Liposome size and size distribution can be controlled to a relatively high degree of monodispersity and can withstand extreme dilutions without variation of the above parameters. ON_1TEG-Chol insertion and distribution within the membranes are ruled by

TABLE 3: Hydrodynamic Radii and Polydispersity Values for POPC Liposome Solution upon Addition of ON_1TEG-Chol 4.1 μM at Different Times

	POPC Liposomes			
	reference sample		with ON_1TEG-Chol 4.1 μM	
time [h]	R_h [Å]	polydispersity	R_h [Å]	polydispersity
1	328 ± 5	0.066	347 ± 5	0.066
2	327 ± 6	0.067	349 ± 5	0.066
6	330 ± 5	0.072	351 ± 6	0.068
24	331 ± 4	0.073	352 ± 5	0.060

thermal equilibrium, which guarantees self-repair from defects that can be generated under kinetic control.

ON_1TEG-Chol has been added to a preformed liposomal suspension (final [POPC]= 1.3 mM) in the concentration range 0.3−52 μM. For the interval 4.1−16 μM hybridization with the complementary strand has also been investigated. As discussed in the previous section, below 15 μM ON_1TEG-Chol is not aggregated.

If the ON_1TEG portion of the molecules protrudes outward from the membrane, the insertion should cause an increase of hydrodynamic radius of the liposomes, due to the added hydrodynamic thickness. This can be monitored using QELS to follow the time evolution of intensity autocorrelation functions. Therefore intensity autocorrelation functions were recorded at different equilibration times after dilution of the vesicular suspension with TBS containing the oligonucleotides, showing, on a log−log scale a slope variation that can be directly correlated with a size variation.

Table 3 reports the hydrodynamic radii and the polydispersity as determined through a second order cumulant fitting of the autocorrelation functions.

The decrease of the decay rate, observed in the autocorrelation functions, corresponds to an increase in hydrodynamic radius with time (column 4, Table 3), until equilibrium is reached within 6 h. The size invariance observed in the reference sample, POPC at the same final concentration and temperature, provides clear-cut evidence that the increase in hydrodynamic radius of the scattering objects is a direct consequence of ON_1TEG-Chol incorporation into liposomes. The observed radius increase corresponds to an increase of the hydrodynamic thickness around the vesicle, due to the hydrophilic portion of the guest molecules. This behavior has been previously observed with DNA-coated polystyrene particles and has been taken as the indication of coupling between the nanoparticle and the single strand oligonucleotide.[48] An interesting observation concerns the small, but reproducible, decrease in polydispersity that follows ON_1TEG-Chol insertion. This rules out that the observed increase in size is due to partial vesicle fusion, which would enlarge size distribution and skew the average size toward higher values. We believe that the origin of this effect lies in the membrane stiffening and in the consequent decrease of thermally activated shape deformation of vesicles.[49]

The gradual achievement of the final hydrodynamic thickness (six hours in this case) can be correlated with the insertion kinetics of ON_1TEG-Chol in the membrane; this means that the final radius of the vesicles decorated by the oligonucleotide is dependent upon the oligonucleotide/lipid ratio. Therefore, we have investigated the equilibrium thickness increase as a function of the added ON_1TEG-Chol. The contribution of the oligonucleotide does not depend on the initial size of the vesicles, whose radius of curvature (330−350 Å) is higher than the fully extended length of the ON_1TEG (≈90 Å).

The concentration of lipophilic oligonucleotides has an unambiguous effect on the equilibrium hydrodynamic size. The increase of hydrodynamic thickness, termed H_0, is reported in Figure 3 as a function of the average distance between grafting sites, calculated as specified in the experimental part. The dependence of the thickness of the hydrodynamic layer on surface coverage indicates a conformational transition of the oligonucleotidic chain as the surface coverage is increased and the average distance between anchoring sites on the vesicular surface is decreased.

The physical properties of polymers and polyelectrolytes grafted to planar and globular surfaces have been the subject of considerable theoretical and experimental efforts. Most of the advances in the field are due to Alexander and De Gennes for neutral polymers[50,51] and to Pincus, Zhulina, and Birshtein,[52,53] among others, for polyelectrolytes, whose high charge density confines counterions in the brush and determines conformational properties totally different from the neutral counterparts. The osmotic pressure due to confined counterions stretches the chains against entropic elasticity. The conformation of the polyelectrolytes results from this balance. The natural gauge to quantify the charge density for a polyelectrolyte is the Manning condensation parameter, ($q_0 = l_B/l$) which compares the charge spacing along the backbone, l, with the solvent Bjerrum length l_B (7.14 Å for water). If this ratio (4.2 for dsDNA, 1−1.7 for ssDNA) is higher than unity, then counterion condensation occurs and renormalizes charge spacing to this distance.

In our experimental conditions the parameters for ssDNA are not unanimously defined in the literature. Several lengths for the monomer size have been reported, varying from 4.3 to 7 Å; moreover the persistence length, between 7.5 Å and 35 Å,[24] is comparable to the monomer size. These data suggest a rather flexible conformation if compared to the dsDNA, which is a very stiff and highly charged polyelectrolyte, with a persistence length of ∼150 base pairs (l_p = 500 Å) in physiological buffer. The significant difference in flexibility, which can be modulated simply by addition of the complementary strand, is in fact one of the most attractive properties of this molecular machinery for supramolecular chemistry.

Even if we are aware that the polyelectrolyte theory is not strictly appropriate for such short oligonucleotides, it is worth to tentatively apply it to our case to infer a characteristic size for the chain protruding from the vesicles.

In view of the previous considerations and of the fact that the relatively high ionic strength should render the brush quasi-neutral, we will consider the segment TEG-ssDNA as a swollen coil characterized by its Flory radius, while we will consider dsDNA as a rigid rod.[54] Therefore the oligonucleotides (either anchored to a bilayer or organized at the air/water interface) will occupy a hemisphere with radius corresponding to the swollen coil Flory radius for the ssDNA or to the contour length for dsDNA. Within these assumptions one can therefore apply the scaling theory[51] describing the conformation of flexible polymer chains grafted to a planar surface and immersed in a good solvent, which predicts the structural state of the polymeric chains. The TEG-18-mer oligonucleotide portion is highly soluble in the aqueous buffer used in this study and the vesicle shell can be reasonably approximated as a planar surface, considering that the particle diameters are very large compared to the maximum chain extension.

Below 15 μM there is a clear dependence of hydrodynamic thickness on surface coverage and the observed trend follows a power law, represented by a linear trend in the double logarithmic plot. For high surface coverage (≥15 μM) this linear

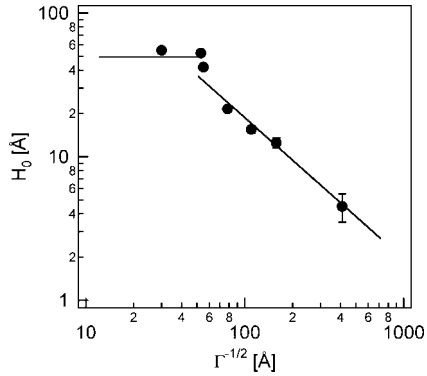

Figure 3. Hydrodynamic thickness H_0 as a function of the average distance between grafting sites $\Gamma^{-1/2}$ for the samples listed in Table 1.

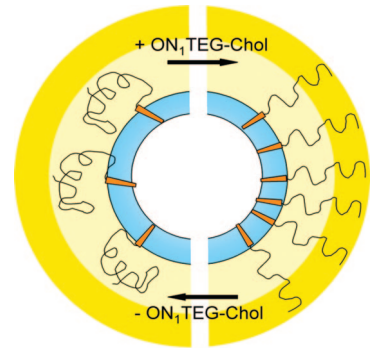

Figure 4. Cartoon of the possible conformational transition of ON_1TEG-Chol grafted onto a POPC liposome surface.

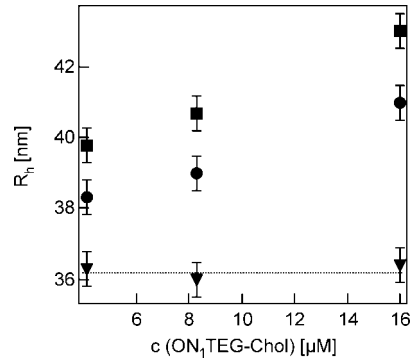

Figure 5. Hydrodynamic radius of liposomes/ON_1TEG-Chol (circles) and liposomes/ON_1TEG-Chol/ON_2-FAM (1:1) (squares) as function of ON_1TEG-Chol concentration. POPC liposomes (triangles) are reported as a reference.

tend is loosened. Even if the low number of high-density data points does not allow us to draw decisive conclusion, this slope change could indicate that the hydrodynamic thickness around the vesicles levels off. A complementary investigation performed using QCM (quartz crystal microbalance) on the adsorption of ON_1TEG-Chol onto a planar POPC bilayers[20] indicates the bilayer saturation beyond a POPC/ON_1TEG-Chol ratio equal to $\leq$80. This value corresponds for vesicles solutions in our esperimental conditions to ON_1TEG-Chol concentrations $\geq$10 μM in agreement with the trend for the hydrodynamic radius reported in Figure 3 (the three data points on the left-hand). We can therefore consider this leveling of the hydrodynamic thicknesses as the approach to the saturation threshold.

By comparing the average distance between grafting sites, $\Gamma^{-1/2}$, to the Flory radius, $R_F = \langle N \rangle^{3/5} a$, (where $\langle N \rangle$ is the degree of polymerization and a the monomer size), given for a coiled chain in a good solvent, two principal regimes have been defined: for $\Gamma^{-1/2} > R_F$, the polymers develop as separate coils or mushrooms, whereas when $\Gamma^{-1/2}$ becomes comparable to R_F, the chains overlap and adopt a stretched state or brush regime. Depending on the monomer length used in the calculations (4.3 or 7 Å), the Flory radius of TEG-ss-18-mer varies from 40 to 55 Å. The distances between anchoring sites are comparable to the Flory diameter and, therefore, we are in a dense brush state and the hydrodynamic thickness should have a scaling-law dependence on the distance between anchoring sites, ($H \approx (\Gamma^{-1/2})^{-2/3}$ for planar surfaces). We obtain a higher scaling exponent (-0.85) for our data. This might be due to the relatively short sequence, for which statistic theories of polymers might not be fully appropriate, as we have already stressed. Nevertheless the dependence of this hydrodynamic thickness on the surface coverage necessarily implies a varied conformational state, as very schematically sketched in Figure 4, which may affect the kinetics as well as the thermodynamics of hybridization with the complementary oligonucleotide. In view of the possible structural application of this molecule to supramolecular architectures on lipid membranes, this feature is of paramount importance and needs to be taken in due account.

Hybridization. Figure 5 shows the increase of the thickness of the hydrodynamic layer discussed above, together with the further increase that is observed upon hybridization. Interestingly, in this case light scattering proves to be a sensitive method to monitor base pairing. The same measurements, performed for the oligonucleotides in solution, without the presence of liposomes, do not yield any appreciable indication that the biorecognition event has occurred. Therefore, liposomes act as amplifier, because in this case hybridization shows up as additional hydrodynamic thickness which adds to fairly strong scatterers.

In hybridization, as far as the brush height is concerned, two opposing mechanisms are acting; on one hand there is a contraction of the basic monomer length, whereas the increased rigidity increases the effective oligonucleotide radius to its contour length.

An interesting point is that the observed increase upon hybridization is practically concentration-independent. We are not currently able to envisage a precise model for this behavior. A possible explanation could be that after hybridization the oligonucleotide is considerably more rigid and the mushroom-brush model does not apply in this case and, therefore, the increase in concentration merely increases the coverage without altering the conformation.

Hybridization can also be followed measuring the electrophoretic mobility. As Figure 6 shows, POPC liposomes have a slightly negative mobility, as commonly reported.[55]

ON_1TEG-Chol insertion is promptly revealed by a shift to more negative ζ-potentials and a broadening of the curve. Hybridization, though characterized by a further broadening, does not cause any further shift. While the brush height is known to increase from QELS, the change in Manning condensation parameter surely alters the thickness of the Gouy−Chapman layer around the vesicles.

Double Strand Melting. We can speculate on the stability of this liposomal hybrid with respect to the adduct in bulk solution through UV absorption, which monitors the hyperchromicity occurring at 260 nm when the two strands come apart upon temperature increase.

We have compared hybridization of ON_1TEG-Chol with its complementary strand in solution and on a liposomal surface

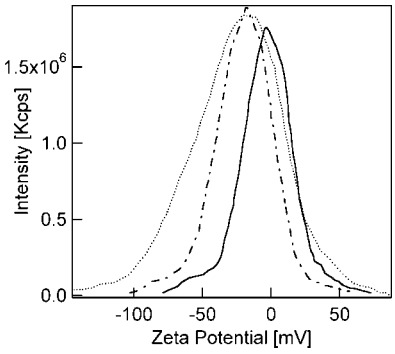

Figure 6. ζ-Potential for POPC liposomes (solid line), POPC/ON_1TEG-Chol, $\langle N \rangle = 125$, (dot-dashed line), and POPC/ON_1TEG-Chol/ON_2-FAM, 1:1 (dotted line).

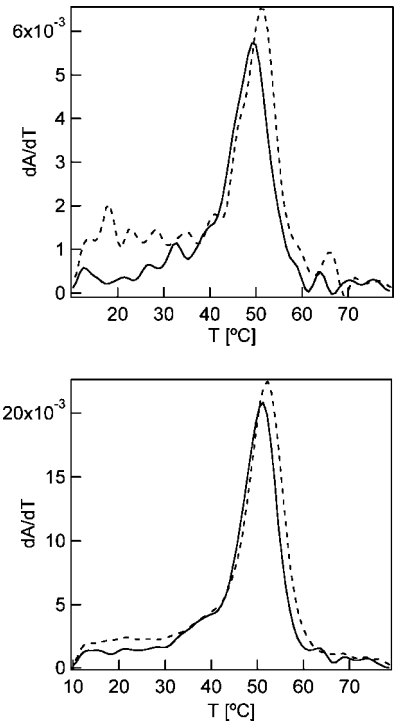

Figure 7. UV melting profiles of ON_1TEG-Chol/ON_2-FAM (1:1) inserted into the liposome (solid curve) and free in solution (dashed curve) for two different oligo concentrations, left 1.1 μM, right 4.1 μM.

for 4.1 μM and 1.1 μM by addition of the pairing strand at room temperature in a 1:1 stoichiometry. As mentioned previously, aggregates are formed above 15 μM and therefore the results for liposomes and solution might not be directly comparable above this threshold. The complementary strand has a FAM label that has been exploited for further fluorescence studies. Figure 7 shows the first derivative of the absorption as a function of temperature for the two different coverages compared to the behavior in solution.

The melting temperature is 2 °C lower (corresponding to a single base mismatch) if the oligonucleotide is anchored onto a liposomal surface. The extent of hyperchromicity is comparable, supporting a substantial equivalence in the two cases. The differences between solution melting and liposomal melting are amplified for the lowest concentration. The full width at half-maximum (fwhm) for the liposomal curve is slightly lower than in solution, suggesting a more cooperative transition in the case of bilayer anchoring. While we are not aware of similar studies in the literature for fluid membranes, some similar studies have been performed for DNA coated gold nanoparticles.[47]

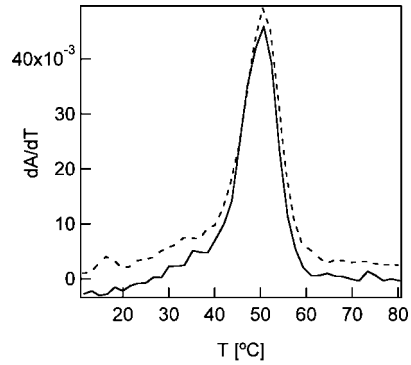

Figure 8. UV melting profile of ON_1TEG-Chol/ON_2 4.1 μM (1:1) inserted into liposomes (solid curve) and free in solution (dashed curve).

The heating−cooling scans have demonstrated that melting is fully reversible. Therefore the liposomal decoration with double strand oligonucleotides can be switched on and off thermally. This characteristic can be exploited in the design of complex architectures, composed of several complementary strands, by tailored programming of melting temperatures, which are predictably correlated to the base sequence.

Before speculating about the origin of such differences, we measured the same curves without the FAM substitution on the complementary strand. Surprisingly the melting curves almost superimpose for both concentrations (as shown below in Figure 8 for 4.1 μM).

Therefore, the differences in melting are solely due to the FAM functionalization on the complementary strand; the fluorophore clearly interacts with the bilayer. However, we should stress that all the measurements for ds-DNA presented in this paper have been performed with the FAM-oligonucleotides and the results should be interpreted with this caveat.

Since QELS has demonstrated to be a sensitive technique for hybridization, it can be used to monitor melting and to ascertain whether the dissociation is reversible.

We measured QELS for POPC, POPC/ON_1TEG-Chol, POPC/ON_1TEG-Chol/ON_2-*FAM* as a function of temperature between 25 and 55 °C (see Figure 9). While we observe the normal progression of the autocorrelation functions (as mentioned above) for the three samples at 25 °C, the curves for POPC/ON_1TEG-Chol and POPC/ON_1TEG-Chol/ON_2-FAM coincide at 55 °C. This result indicates that melting causes the complete detachment of ON_2-FAM from the vesicular surface. Going back to 25 °C, the situation illustrated is fully recovered, demonstrating that the thermoresponsivity is completely reversible.

Comparing the melting curves of POPC/ON_1TEG-Chol/ON_2-FAM at different temperatures, renormalized for T variation, we notice that the trend of the hydrodynamic radius is not monotonic.

Some authors have recently demonstrated[56] by using SANS that oligonucleotide single strands have a pronounced conformational dependence on temperature. Therefore, the T-dependence superimposes and partially annihilates the expected hydrodynamic radius decrease. This bias disappears if one compares POPC/ON_1TEG-Chol and POPC/ON_1TEG-Chol/ON_2-FAM at the same temperature after the melting.

Linear Dichroism. To further prove this conformational transition, we have performed linear dichroism experiments on shear flow deformed POPC/ON_1TEG-Chol and POPC/ON_1TEG-Chol/ON_2-FAM liposomes as a function of the oligonucleotide concentration. LD spectra for three different ON_1TEG-Chol

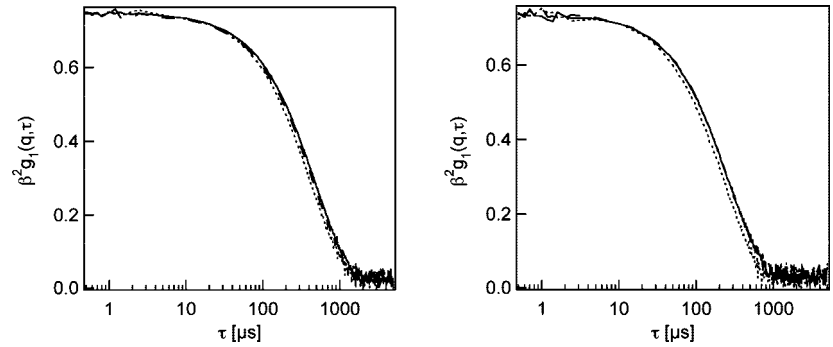

Figure 9. Melting of oligonucleotides as seen with QELS. Left, scattered field autocorrelation functions recorded at room temperature for POPC liposomes, POPC/ON_1TEG-Chol ($\langle N \rangle = 125$), POPC/ON_1TEG-Chol/ON_2-FAM ($\langle N \rangle = 125$). Right: the same autocorrelation functions recorded at 55 °C, after storage of the samples at 55 °C for 2 h.

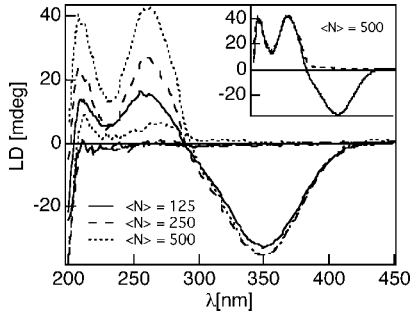

Figure 10. LD Spectra of ON_1TEG-Chol (lower signals) and ON_1TEG-Chol/ON_2-FAM incorporated in flow deformed POPC liposomes as a function of ON_1TEG-Chol concentration. LD spectra of the sample at $\langle N \rangle = 500$ before and after the addition of retinoic acid are shown in the inset. Solid line $\langle N \rangle = 125$, dashed line $\langle N \rangle = 250$, dotted line $\langle N \rangle = 500$. ON_1TEG-Chol/ON_2-FAM ratio is 1:1.

concentrations before and after the hybridization are reported in Figure 10.

Control measurements done at the same concentrations and the same shear rates in solution yield no signal, meaning that the oligonucleotide portion is too short to align under flow.

Therefore possible preferential alignment by shear of base chromophores is provided by their liposomal anchoring.

The signals for POPC/ON_1TEG-Chol liposomes (single strand DNA chains) are very low, except for the slight positive signal of the most concentrated sample ($\langle N \rangle = 500$, $\Gamma^{-1/2} = 55$ Å). This indicates that for $\langle N \rangle = 250$ and $\langle N \rangle = 125$, ss-DNA chains are basically randomly oriented with respect to the shear direction (i.e., lipid surface) and confirms that the assumption of a random coil conformation, done in the previous paragraphs, was substantially correct. Nevertheless, when liposomal coating is increased, the occurrence of a stronger positive signal can be interpreted as due to the conformational transition which induces the oligonucleotide to adopt a preferred orientation with respect to the bilayer, with the long axis sticking out from the membrane. This result agrees with the observed rise of hydrodynamic radius observed in QELS experiments upon ON_1TEG-Chol addition.

However, the most striking variation comes as an effect of hybridization of the complementary strand. It is evident that the addition of the complementary sequence (ON_2-FAM) induces a strong change in DNA orientation with respect to the lipid surface as denoted by the marked increase of the signal, irrespectively of concentration. Therefore upon hybridization we observe the transition from quasi-random coil ss-DNA to rigid ds-DNA rod, confirming the trend observed in light scattering.

In particular, the increase in the positive signal indicates that DNA, upon hybridization, slightly rises from the membrane surface. A qualitative evaluation of the tilt angle can be deduced calculating the angle α (the angle between the macroscopic axis and the transition moment of the chromophore)[36] and knowing that the resultant of the bases transition moments is perpendicular to the double helix molecular axis.

The orientation parameter of the liposomes, S, can be evaluated from the retinoic acid, for which $\alpha = 90°$. The LD spectra for $\langle N \rangle = 500$ before and after the addition of retinoic acid are shown in the inset of Figure 10. The incorporation of retinoic acid into the membrane, indicated by the presence of the large negative band centered at 350 nm, does not affect the positive DNA signal at 260 nm and hence does not influence its orientation with respect to the membrane. We have estimated a tilting angle of DNA duplex of about 45−46° with respect to the lipid surface. The invariance of the tilt angle with the coating is in line with QELS results, where the additional increase of hydrodynamic thickness due to hybridization appears concentration-invariant.

Hybridization Kinetics. As shown in the previous paragraphs, the ON_1TEG-Chol density on the bilayer determines different conformations of the single strand chain at the surface. We could now speculate how the different chain configurations can affect the kinetics of hybridization.

Previous kinetic studies of immobilized DNA hybridization have mainly focused on planar solid supports for the obvious implications in microarray-based technology. Hybridization rates have been found to increase at lower oligonucleotide surface densities.[57]

An important aspect is the comparison with the hybridization in solution: it has been shown that the associative kinetics of surface DNA hybridization on planar gold surface are suppressed by a factor of 20 to 40-fold compared to solution-phase hybridization[58] and a 5- to 10-fold suppression in hybridization rates of 22mers is also observed on microparticles by means of FRET measurements.[59]

To the best of our knowledge, no such studies have ever been performed on hard or soft nanoparticles, where the radius of curvature compares with the contour length of the oligonucleotide.

To this purpose, we have performed UV stopped-flow absorption spectroscopy for a series of vesicle/oligonucleotide hybrids at different POPC/oligonucleotide ratios ($\langle N \rangle$), by varying the lipid concentration, while keeping the ss-oligo *nucleotide* concentration constant at 2 μM. Hybridization between ON_1TEG-Chol incorporated into the vesicles and the complementary strand ON_2 free in solution was monitored as a

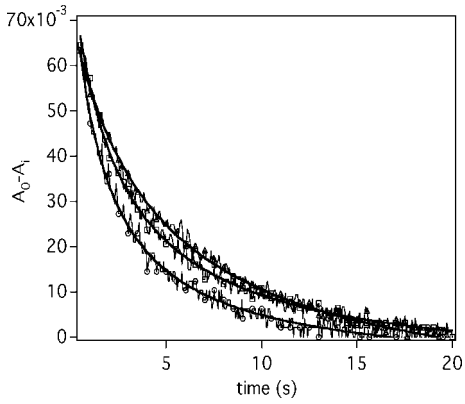

Figure 11. Kinetics of ON_1TEG-Chol/ON_2 hybridization onto POPC vesicles at three different POPC/ON_1TEG-Chol molar ratios: 82 (triangles), 164 (squares), and 657 (circles).

decrease in UV absorbance at 260 nm, upon rapid mixing of equal molar concentrations of the two oligonucleotide solutions in TBS.

Strand pairing is generally accepted as consisting of two sequential processes, i.e., initial formation of a nucleation complex, followed by the zippering of the duplex.[60] The initial association complex can dissociate or seal, depending on the temperature. For relative short segments, up to several hundred base pairs, nucleation is the rate-determining step at low concentrations.

The time course of the absorbance, reported in Figure 11, can be well accounted for by the following second-order equation

$$A_t = A_0 + (A_\infty - A_0)\frac{C_0 k_{on} t}{1 + C_0 k_{on} t} \qquad (3)$$

where A_t is the absorbance at time t, A_0 is the absorbance of the ssDNA at $t = 0$, A is the absorbance of the ds-DNA at equilibrium and C_0 is the initial concentration of ssDNA and k_{on} is the rate constant.

The same equation has been applied to oligonucleotides freely diffusing in solution (i.e., the reference sample) and in liposomal suspension. In both cases, the expression describing a second order reaction with equal concentrations of the reactants (ON_1TEG-Chol and ON_2) resulted in the best fit.

Figure 12 reports the results for the rate constants for six samples, differing for grafting densities, while the dashed line represents the comparison with the bulk rate constant. A clear increasing trend for the pairing rate can be observed: as [POPC]/[ON_1TEG-Chol] ratio is increased, hence as oligonucleotide grafting density is decreased, the association rate increases. However, the fact that for liposomal suspensions the rate constants have a monotonous trend indicates that the vesicle diffusion is not rate-determining, and that, comparing different liposomal loadings, other mechanisms determine the nucleation of the double strand complex. This behavior can be explained, in analogy with the microarray case, on the basis of the increased electrostatic repulsion at high surface density of oligonucleotides, that may hinder the association with the complementary strand. Another subtler aspect could affect the hybridization, i.e. the conformation of the single stranded oligonucleotides at the surface, closely connected to the anchorage density. As we have seen, the oligonucleotides at the vesicular surface undergo a conformational transition from mushroom to brush state when the average distance between grafting sites, $\Gamma^{-1/2}$, becomes

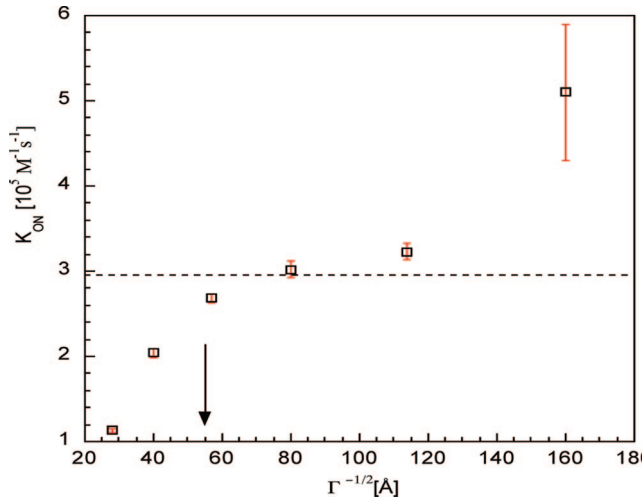

Figure 12. Rate constants dof ON_1TEG-Chol /ON_2 hybridization onto POPC vesicles as a function of the grafting density. The dotted line represents the bulk rate constant.

comparable to the Flory radius, which is in the range from 40 to 55 Å (indicated by the arrow on the x-axis in Figure 12).

If compared to the oligonucleotide kinetic rate in solution, we can see that at about 110 duplexes per vesicle, the rate constant of the oligonucleotide hybridization at the vesicular surface is lower, while below this threshold concentration, the rate constant of hybridization on the vesicle becomes faster than in solution. The 18-mer oligonucleotide can hybridize with the complementary strand faster on the vesicle than in solution, provided grafting density is not too high and roughly lower than the Flory radius. Increasing surface concentration, the denser packing of the oligonucleotides inside the brush may hamper hybridization with complementary strand with respect to the mushroom state, where oligonucleotide chains develop as separate coils.

The advantage of having nanoparticles rather than solid planar supports in the hybridization kinetics relies on the diffusion of these particles that could kinetically favor the association of the incorporated oligonucleotides with the strands in solution. Also, noncovalent anchorage of oligonucleotides to vesicles, rather than covalent linkage to solid supports or microparticles, allows more flexibility and mobility of the grafted molecules onto the surface. Oligonucleotides can rearrange and change their distribution or their relative position on the vesicle, through lateral motion of the cholesterol within the lipid bilayer. This improves as well the association kinetics with a complementary strand in solution. In addition, the conformation of the anchored oligonucleotide is, as previously discussed, an important aspect in the hybridization kinetics: the threshold POPC/ON_1TEG-Chol ratio at which hybridization on the vesicles becomes faster than in solution corresponds to a calculated average grafting site distance of $\sim$ 50 Å, which is comparable to the Flory radius of the ON_1TEG. This might be interpreted as if the main factor controlling the kinetic properties is the conformation at the surface. This is a very promising result in order to fabricate efficient nanosystems for DNA recognition and self-assembly.

Conclusions

This paper reports an investigation of the surface tension and aggregation properties of the ON_1TEG-Chol oligonucleotide derivative. This derivative forms aggregates in aqueous solution (TRIS 50 mM, NaCl 100 mM) above 15 μM, as inferred from surface tension, quasi elastic light scattering and pyrene emission behavior.

The spontaneous insertion in a curved lipid bilayer is detected as an increase of hydrodynamic thickness of the liposome by means of QELS. The insertion proceeds until the grafting density is comparable with ON_1TEG-Chol radius ($\langle N \rangle = 500$). The conformation of the hydrophilic part (ON_1TEG), sticking out from the lipid membrane, is strongly dependent upon the average distance between anchoring sites onto the vesicular surface, passing from a quasi-random coil to a more rigid configuration as surface coverage increases, as inferred from QELS and linear dichroism (LD) results.

The oligonucleotide anchored to the liposomal surface efficiently and reversibly binds its complementary strand in solution. Both light scattering and LD proved to be sensitive methods to selectively detect the hybridization in the presence of liposomes that act as amplifiers of the observed signal in the first case and as shear-aligned hosts in the second case.

Most of the oligonucleotide properties, from conformation to hybridization kinetics, can be controlled by surface density, i.e. by varying the lipid/*oligonucleotide* ratio.

Liposomes with single strand and double strand decoration remain stable within the experimental time window (about one week). This structure represents a successful and stable amphiphile/DNA supramolecular hybrid, where a DNA guest is inserted into a membrane thanks to hydrophobic interactions. ON_1TEG-Chol is therefore a suitable building block that can effectively serve as a hydrophobic anchor into fluid bilayer to assemble supramolecular constructs based on DNA digital code.

Acknowledgment. The authors acknowledge EU-STREP program (Project reference AMNA, Contract No 013575), PRIN 2006 and CNR-FUSINT for financial support. Dr. Claudiu Supuran and Dr. Alessio Innocenti are acknowledged for help in the Stopped Flow Experiments.

Supporting Information Available: Text and a table of surface tension meausrements. This information is available free of charge via the Internet at http://pubs.acs.org.

References and Notes

(1) Gelbart, W. M.; Ben-Shaul, A. *J. Phys. Chem.* **1996**, *100*, 13169.
(2) Lehn, J. M. *Supramolecular Chemistry: Concepts and Perspectives*; Wiley: New York, 1995.
(3) Bonini, M.; Berti, D.; Di Meglio, J. M.; Almgren, M.; Teixeira, J.; Baglioni, P. *Soft Matter* **2005**, *1*, 444.
(4) Berti, D. *Curr. Opin. Colloid Interface Sci.* **2006**, *11*, 74–78.
(5) Feldkamp, U; Niemeyer, C. M. *Angew. Chem., Int. Ed.* **2006**, *45*, 1856–1876.
(6) Tumpane, J.; Sandin, P.; Kumar, R.; Powers, V. E. C.; Lundberg, E. P.; Gale, N.; Baglioni, P.; Lehn, J.-M.; Albinsson, B.; Lincoln, P.; Wilhelmsson, L. M.; Brown, T.; Norden, B. *Chem. Phys. Lett.* **2007**, *440*, 125–129.
(7) Berti, D.; Baglioni, P.; Bonaccio, S.; Luisi, P. L. *J. Phys. Chem. B* **1998**, *102*, 303.
(8) Berti, D.; Barbaro, P; Bucci, I.; Baglioni, P. *J. Phys. Chem. B* **1999**, *103*, 4916–4922.
(9) Baglioni, P; Berti, D. *Curr. Opin. Colloid Interface Sci.* **2003**, *8*, 55–61.
(10) Baldelli Bombelli, F.; Berti, D.; Pini, F.; Keiderling, U.; Baglioni, P. *J. Phys. Chem. B* **2004**, *108*, 16427–16434.
(11) Baldelli Bombelli, F.; Berti, D.; Keiderling, U.; Baglioni, P. *J. Phys. Chem. B* **2002**, *106*, 11613–11621.
(12) Banchelli, M.; Berti, D. Baglioni, P. *Angew. Chem., Int. Ed.* **2007**, *46*, 3070–3073.
(13) Milani, S.; Baldelli Bombelli, F.; Berti, D.; Baglioni, P. *J. Am. Chem. Soc.* **2007**, *129*, 11664–11665.
(14) Mirkin, C. A.; Letsinger, R. L.; Mucic, R. C.; Storhoff, J. J. *Nature* **1996**, *382*, 607.
(15) Alivisatos, A. P.; Johnsson, K. P.; Peng, X. G.; Wilson, T. E.; Loweth, C. J.; Bruchez, M. P.; Schultz, P. G. *Nature* **1996**, *382*, 609.
(16) Xu, C.; Taylor, P.; Fletcher, P. D. I.; Paunov, V. N. *J. Mater. Chem.* **2005**, *15*, 394–402.
(17) Pfeiffer, I.; Hook, F. *J. Am. Chem. Soc.* **2004**, *126*, 10224.
(18) Yoshina-Ishii, C.; Miller, G. P.; Kraft, M. L.; Kool, E. T.; Boxer, S. G. *J. Am. Chem. Soc.* **2005**, *127*, 1356.
(19) Shohda, K.; Toyota, T.; Yomo, T.; Sugawara, T. *ChemBioChem.* **2003**, *4*, 778–781.
(20) Banchelli, M.; Gambinossi, F.; Brown, T.; Caminati, G; Berti, D.; Baglioni, P. Manuscript in preparation 2008.
(21) Erkan, Y.; Czolkos, I.; Jesorka, A.; Wilhelmsson, L. M.; Orwar, O. *Langmuir* **2007**, *23*, 5259–5263.
(22) Erkan, Y.; Halma, K.; Czolkos, I.; Jesorka, A.; Dommersnes, P.; Kumar, R.; Brown, T.; Orwar, O. *Nano Lett.* **2008**, *8*, 227–231.
(23) Hansen, P. L.; Cohen, J. A.; Podgornik, R.; Parsegian, V. A *Biophys. J.* **2003**, *84*, 350.
(24) Smith, S. B.; Cui, Y. J.; Bustamante, C. *Science* **1996**, *271*, 795–799.
(25) Strick, T. R.; Dessinges, M. N.; Charvin, G.; Dekker, N. H.; Allemand, J. F.; Bensimon, D.; Croquette, V. *Rep. Prog. Phys.* **2003**, *66*, 1–45.
(26) Mills, J. B.; Vacano, E.; Hagerman, P. J. *J. Mol. Biol.* **1999**, *285*, 245–257.
(27) (a) Caruthers, M. H. *Science* **1985**, *230*, 281. (b) Mullis, K. B. *Angew. Chem.* **1994**, *106*, 1271. (c) Mullis, K. B. *Angew. Chem., Int. Ed.* **1994**, *33*, 1209.
(28) Walde, P.; Ichikawa, S. *Biomol. Eng.* **2001**, *18*, 143–177.
(29) Hamilton, J. A. *Curr. Opin. Lipidology* **2003**, *14*, 263–271.
(30) ZanaR. *In Surfactant Solutions: New Methods of Investigation*; Zana,R., Ed.; Marcel Dekker: New York, 1987; pp 241−294..
(31) Fry, D. W.; White, C.; Goldman, D. J. *Anal. Biochem.* **1978**, *90*, 809.
(32) Barrow, D. A.; Lentz, B. R. *BBA* **1980**, *597*, 92.
(33) Kalyanasundaram, K.; Thomas, K. *J. Am. Chem. Soc.* **1977**, *99*, 2039.
(34) Ardhammar, M.; Lincoln, P.; Norden, B. *Proc. Nat. Acad. Sci. U.S.A.* **2002**, *99*, 15313–15317.
(35) Ardhammar, M.; Mikati, N.; Norden, B. *J. Am. Chem. Soc.* **1998**, *120*, 9957–9958.
(36) Rajendra, J.; Damianoglou, M.; Hicks, P.; Booth, P.; Rodger, P. M.; Rodger, A. *Chem. Phys.* **2006**, *326*, 210–220.
(37) Svensson, F. R. J.; Lincoln, P.; Norden, B.; Esbjorne, E. K. *J. Phys. Chem. B* **2007**, *111*, 10839−10848.
(38) Brattwall, C. E.; Lincoln, P.; Norden, B. *J. Am. Chem. Soc.* **2003**, *125*, 14214–14215.
(39) Mukhopadhyay, S.; Maitra, U. *Curr. Sci.* **2004**, *87*, 1666–1683.
(40) Ninomiya, R.; Matsuoka, K.; Moroi, Y. *Biochim. Biophys. Acta* **2003**, *1634*, 116–125.
(41) Dar, A. A.; Chatterjee, B.; Rather, G. M.; Das, A. R. *J. Colloid Interface Sci.* **2006**, *298*, 395–405.
(42) Tedeschi, C.; Mohwald, H.; Kirstein, S. *J. Am. Chem. Soc.* **2001**, *123*, 954–960.
(43) Tirado, M. M.; Martinez, C. L.; De La Torre, J. G. *J. Chem. Phys.* **1984**, *81*, 2047.
(44) Seeman, N. C. *Nature* **2003**, *421*, 427.
(45) Mirkin, C. A. *Inorg. Chem.* **2000**, *39*, 2258.
(46) Xu, J.; Craig, S. L. *Langmuir* **2007**, *23*, 2015–2020.
(47) Xu, J.; Craig, S. L. *J. Am. Chem. Soc.* **2005**, *127*, 13227–13231.
(48) Cardenas, M.; Schillen, K.; Pebalk, D.; Nylander, T.; Lindman, B *Biomacromolecules* **2005**, *6*, 832–837.
(49) Joannic, R.; Auvray, L.; Lasic, D. D. *Phys. Rev. Lett.* **1997**, *78*, 3402–3405.
(50) Alexander, S. *J. Phys. (Paris)* **1977**, *38*, 938.
(51) De Gennes, P. G. *Macromolecules* **1980**, *13*, 1069–1075.
(52) Witten, T. A.; Pincus, P. *Europhys. Lett.* **1987**, *3*, 315.
(53) Birshtein, T. M. *J. Phys. II Fr.* **1992**, *2*, 63–74.
(54) Turner, D. H. In *Nucleic Acids: Structures, Properties and Functions*; Bloomfield, V. A. C. D. M.,Tinoco, I., Jr., Ed.; University Science Press: Mill Valley, CA,2000.
(55) Liu, D. Z.; Chen, W. Y.; Tasi, L. M.; Yang, S. P. *Colloid Surface A* **2000**, *172*, 57–67.
(56) Zhou, J.; Gregurick, S. K.; Krueger, S.; Schwarz, F. P *Biophys. J.* **2006**, *90*, 544–551.
(57) Peterson, A. W.; Heaton, R. J.; Georgiadis, R. M. *Nucleic Acid Res.* **2001**, *29*, 5163.
(58) Gao, Y.; Wolf, L. K.; Georgiadis, R. M. *Nucleic Acid Res.* **2006**, *34*, 3370–3377.
(59) Henry, M. R.; Stevens, P. W.; Sun, J.; Kelso, D. M. *Anal. Biochem.* **1999**, *276*, 204–214.
(60) Wetmur, J. G.; Davidson, N. *J. Mol. Biol.* **1968**, *31*, 349–370.

JP802415T